

Interpretation of Seismic Tests

Massarsch, K.R.⁽¹⁾, Noel Perez⁽²⁾, Terceros A. M.⁽²⁾ and Terceros H. M. A.⁽²⁾

⁽¹⁾Geo Risk & Vibration AB, Bromma, Sweden. <rainer.massarsch@georisk.se>

⁽²⁾ Incotec S.A., Santa Cruz de la Sierra, Bolivia <mta@incotec.cc>, <math@incotec.cc>
<noel.perez@incotec.cc>

ABSTRACT. Comprehensive geotechnical and seismic investigations have been carried out at the B.E.S.T. site. The following tests were performed: seismic refraction, surface wave measurements (MASW) and seismic down-hole tests (one and two sensors). The investigations offer a unique opportunity to compare the results of the different seismic tests at a relatively homogeneous site. The effect of strain softening on the shear modulus is accounted for by the introduction of a modulus reduction factor. Geotechnical parameters such as plasticity index, void ratio and degree of saturation influence the modulus reduction factor. A concept is presented which makes it possible to estimate the soil modulus at large strain. The results of shear wave velocity measurements by different methods are compared. The shear modulus and elastic modulus at large strain (static modulus) is estimated.

1. GEOTECHNICAL SETTING

The geology of the B.E.S.T. site is characterized by a sedimentary basin. The soil deposit is the result of a sedimentation-erosion-sedimentation process, dominated by fine to medium sands with intermittent layers of silt, clay or clayey sand. The results of SPT investigations and laboratory soil classification at test point C1 are shown in Figure 1.

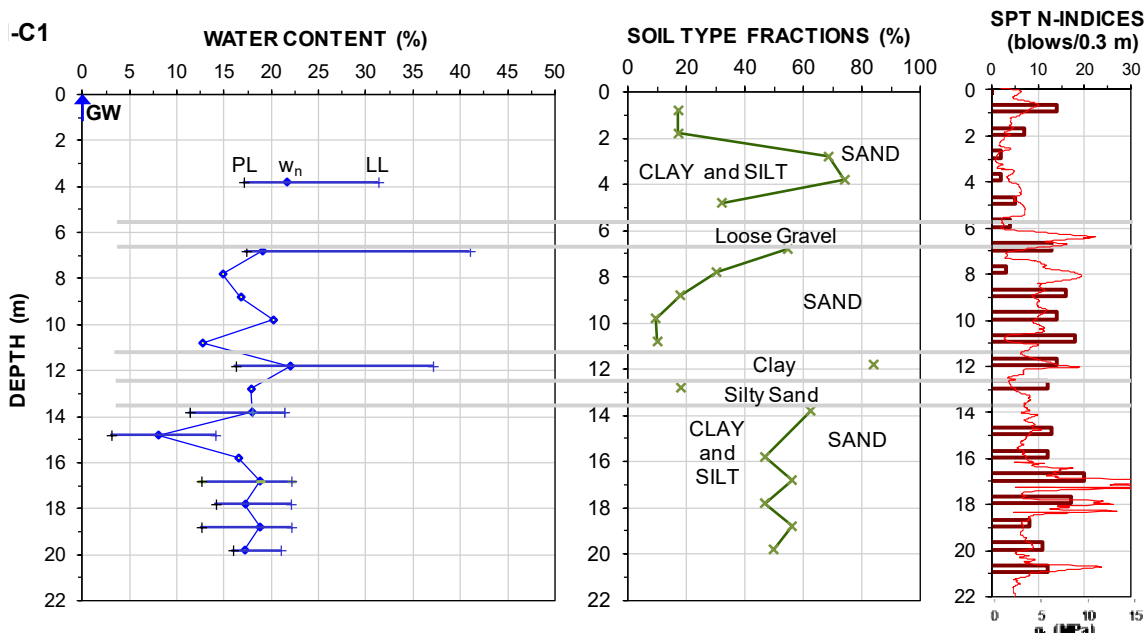


Fig. 1. Results of SPT investigation and soil classification in borehole C1.

The upper about 20 m thick soils consist of normally consolidated layers of clay, silt, and sand, in various combination and thickness. The upper about 5 to 6 m consists of loose silt and sand. Hereunder lies a 6 to 7 m layer of compact silt and sand. At about 11 m depth exists an about 1 m thick layer of soft silty clay followed by an about 1 m thick layer of compact sand. Below about 12 m depth, the profile alternates between about 2 m thick layers of compact to dense silty sand and about 2 m thick layers of loose sand. The groundwater table at the site ranges seasonally between the ground surface and about 0.5 m depth.

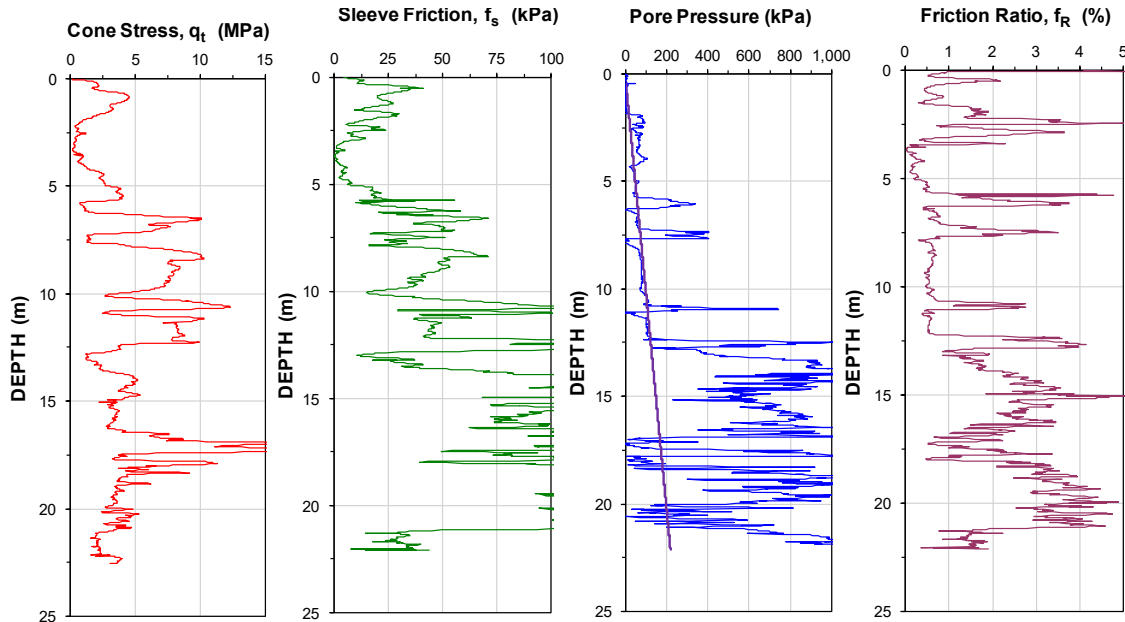


Fig. 2. Results of CPTU at tests pile location C1.

The results of the borehole records and the CPTU from Location C-1 show reasonable agreement. However, the CPTU provides significantly more detailed information. The cone stress shows four general soil layer formations (0–6 m; 6–12.5 m, 12.5–16.5 m and 16.5–22 m), and the pore water pressure measurements add additional valuable information. Down to about 12.5 m, the soil is relatively free-draining, with occasional fine-grained layers. Below 15.5 m, the deposit changes to mainly fine-grained soil. The relatively stiff/dense soil layer between 12.5 and 16.5 m is characterized by negative pore water pressure, indicating a dilative behavior. Different types of seismic measurements were performed at individual locations (SCPT and SDMT) as well as along three profiles. Figure 3 shows an overview of the B.E.S.T. site with test location and seismic profiles (MASW and refraction).

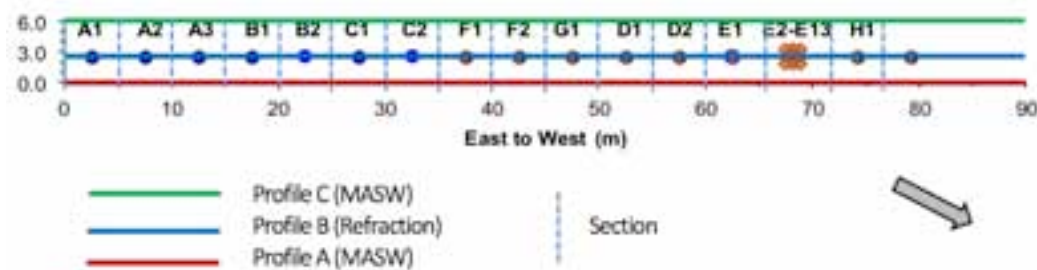


Fig. 3. Test area showing of test piles (Ax-Hx) and seismic profiles (A, B and C).

Seismic tests (MASW and refraction) were performed along three approximately 80 m long profiles (A, B and C). At each test pile location (Ax through Hx), geotechnical (SPT, CPTU, DMT) and seismic tests (SCPT and SDMT) were performed at a distance of 0.8 m from the center of the pile, as illustrated at Location A-1 shown in Figure 4.

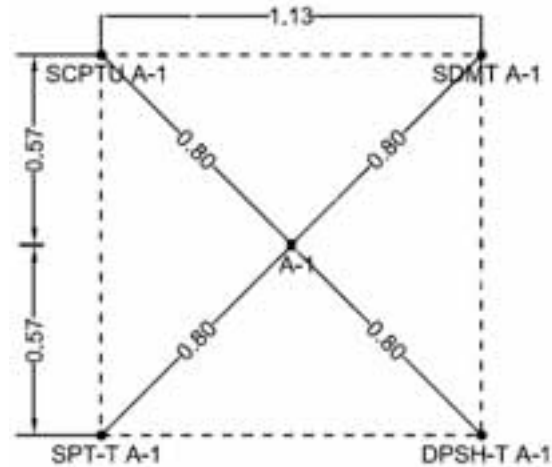


Fig. 4. Location of geotechnical (SPT, DPSH, CPTU and DMT) and seismic tests (SCPT and SDMT), illustrated at Location A-1.

2. SEISMIC TESTING METHODS

Seismic methods have been used extensively within earthquake engineering but are also used increasingly for the solution of geotechnical problems. An important reason has been the rapid development of powerful electronic measurement systems suitable for use under difficult site conditions. Further, the analytical capacity of programs, which can be operated on conventional computers has increased significantly. In the following, the four seismic methods used as part of the investigation are briefly described. For more details, reference is made to publications by e.g., Richart et al. (1970), Santamarina et al. (2001), and Stokoe et al. (2004).

There are two types of seismic body waves, pressure or compression waves (P-waves) as well as shear waves (S waves), and seismic sensors react to both. The P-wave always arrives first. In soils below the groundwater table, the P wave typically travels 2 or more times faster than the S-wave, so separation of the two body waves is easy. Above the water table, however, the difference is small and separation of P- and S-waves may be very difficult, requiring specialized techniques. However, the most significant difference between P- and S-waves is that S-waves are reversible. Therefore, using a source that can produce shear waves of opposite polarity facilitates the identification of S-waves. Since shear waves travel through the skeletal structure of the soil at very small strains, one can apply simple elastic theory to calculate the average elastic small strain shear modulus, over the length interval of measurement, as the mass density times the square of the shear wave velocity. Thus, the shear wave velocity relates directly to stiffness (Massarsch 2004) and may also be used to estimate liquefaction susceptibility in young uncemented sands (Youd et al. 2001).

2.1 Seismic Refraction Method

Seismic refraction has been the most commonly used method in geophysical site exploration and earthquake engineering. However, due to its limitations, it has been replaced by more suitable methods for the solution of geotechnical and soil dynamics problems. In this method, a series of receivers, usually geophones, are placed in a linear array. An energy source (hammer blow or small explosive charge) is then used to generate compression waves, cf. Figure 3. Vertically sensitive geophones are installed at increasing distance, d , from the source, P to record the arrival of compression waves which propagate along soil or rock layers of varying thickness H , cf. Figure 3.

The first arrival of the waves is recorded by the geophones. A fundamental assumption of the refraction method is that the compression wave velocity increases with depth. This requirement imposes an important limitation of the method, as in many geological formations, soft or loose soil layers with lower velocity can occur below a high-velocity layer.

At geophones located close to the point of impact, such as point $G1$, the direct waves reach first. At the points located away from the source, the refracted waves arrive earlier than the direct waves, Figure 5.

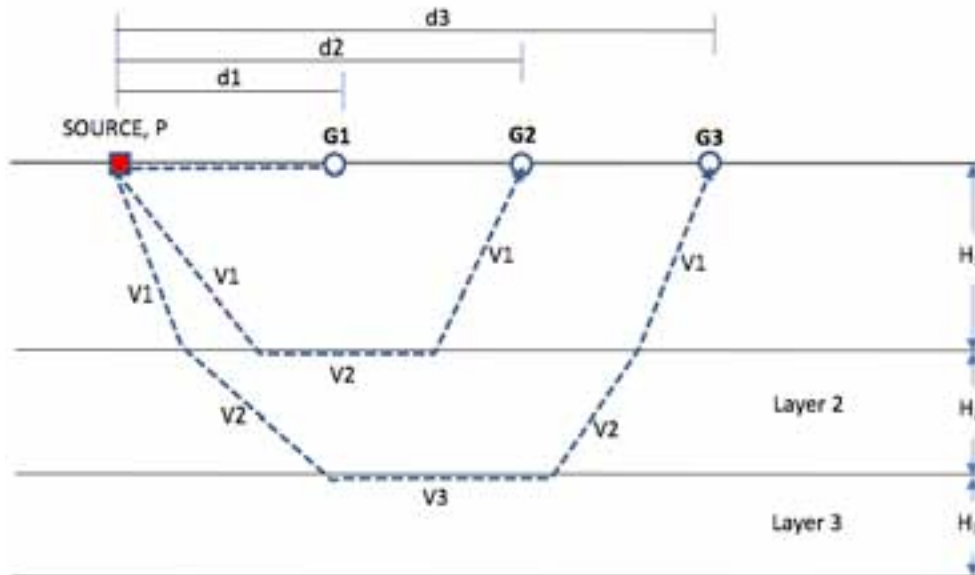


Fig. 5. Arrangement of vertically sensitive sensors (G) and source (P) at seismic refraction test.

From the recorded first arrival of compression waves, the time-distance relation can be plotted, Figure 6. The time, t , of arrival of the first impulse at various geophones is taken as ordinate and the distance, d , of the geophones from the source P is taken as abscissa. Velocity in any layer is equal to the reciprocal of the slope of the corresponding line. The slopes of the various lines are determined, from which the corresponding velocities are computed.

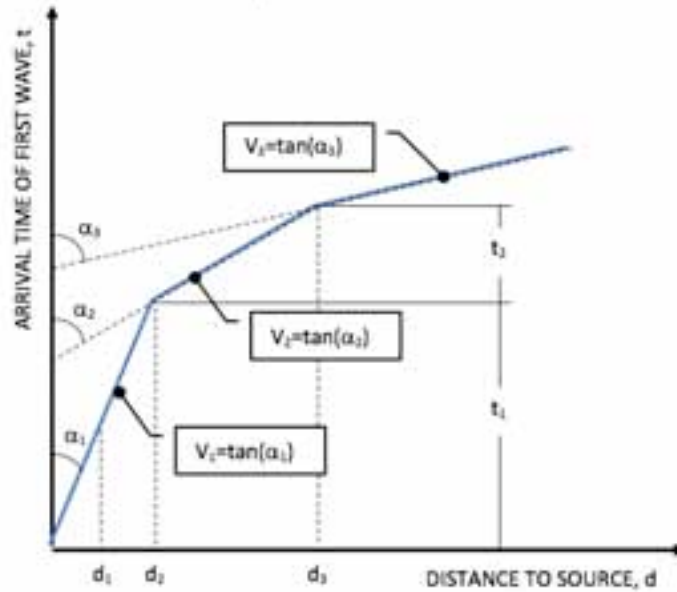


Fig. 6. Time-distance plot of seismic refraction test, cf. Figure 3.

After the determination of velocities at different layers, its depth can be calculated from the following equations:

$$H_1 = \frac{d_1}{2} \sqrt{\frac{V_2 - V_1}{V_2 + V_1}} \quad (1)$$

$$H_2 = 0.85 H_1 + \frac{d_2}{2} \sqrt{\frac{V_3 - V_2}{V_3 + V_2}} \quad (2)$$

It should be noted, that the above case is limited to level ground and gradually increasing wave velocities. More sophisticated, computer-based, analytical models are available.

2.2 Seismic Down-hole Method

Seismic cross-hole and down-hole methods have been widely used soil dynamics and geotechnical earthquake engineering since the beginning of the 1960s. The down-hole method is most widely used today due to the incorporation of seismic sensors in the cone penetration test—the seismic cone penetrometer (SCPT). The seismic down-hole method has been described in the geotechnical literature, (Robertson et al. 1986). Standards and guidance documents have been developed, such as the ISSMGE Guideline “Seismic cone downhole procedure to measure shear wave velocity”, which is attached to this document, (Butcher et al. 2015).

During a pause in cone penetration, a shear wave can be created at the ground surface that will propagate into the ground on a hemispherical front and a measurement made of the time taken for the seismic wave to propagate to the seismometer in the cone. By repeating this measurement at another depth, one can determine, from the signal traces, the interval time and so calculate the average shear wave velocity over the depth interval between the seismometers. A repetition of this procedure with cone advancement yields a vertical profile of vertically propagating shear wave velocity. The general arrangement of SCPT equipment is shown in Figure 7.

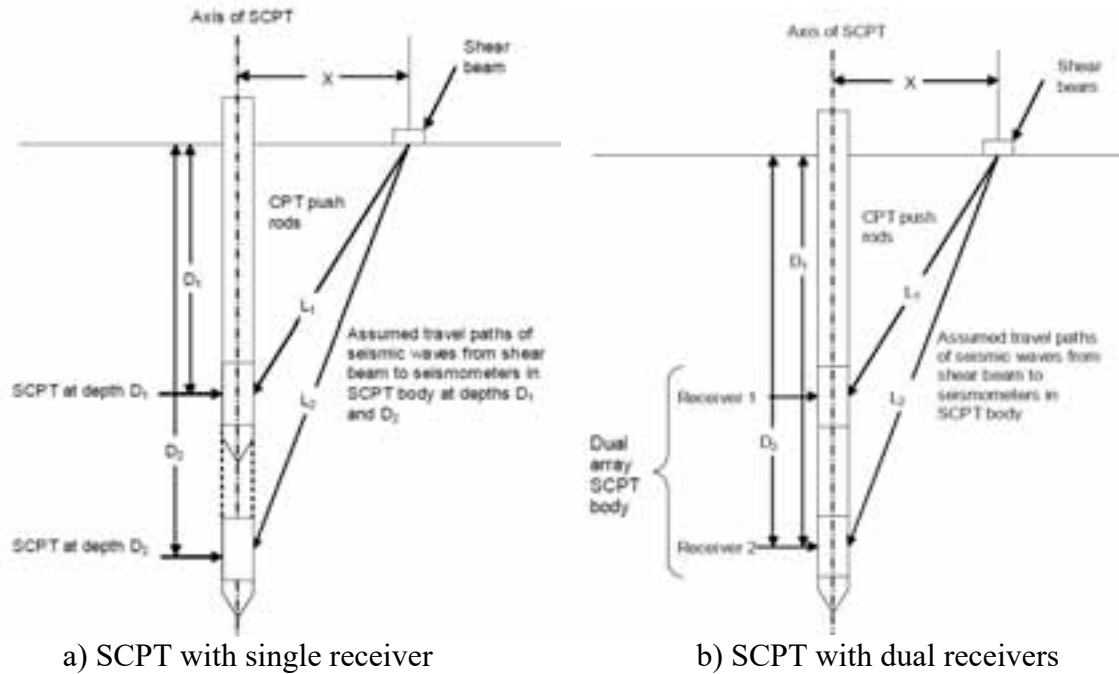


Fig. 7. Schematic diagram of SCPT with single and dual seismic sensors, (Butcher et al. 2015).

Figure 8 illustrates the execution of a seismic down-hole test (SDMT) at the B.E.S.T. site. A horizontally polarized shear wave is generated by striking a steel plate (loaded by the CPT rig). A trigger activates the recording equipment that then displays the time based signal trace received by the seismometer.



Fig. 8. Execution of a seismic down-hole test (SDMT) at the B.E.S.T. site, courtesy Incotec.

An example of a pair of signals is shown in Figure 9. With reversed image traces, the first major cross-over can be taken as the “reference” arrival, or one trace may be used and an arrival pick made visually by an experienced operator. Alternately, a cross-correlation procedure may be used to find the interval travel time using the wave traces from strikes on the same side at successive depths. The latter technique is more complex, but eliminates the arbitrary visual pick of arrival time and is necessary if symmetry of reverse wave traces is lacking.

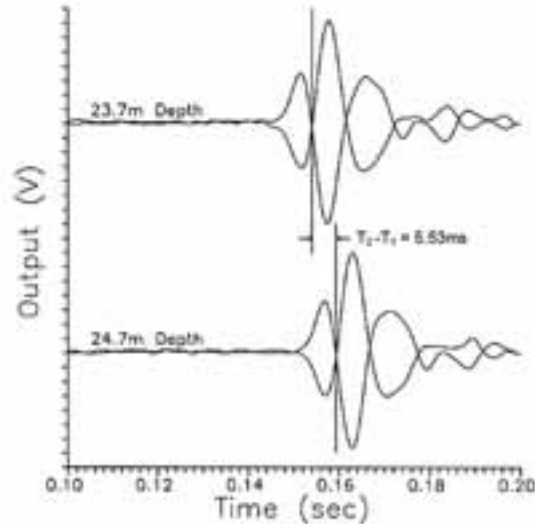


Fig. 9. An example of oppositely polarized shear wave traces with clear crossover of traces showing the interval time $T_2 - T_1$. (Butcher et al. 2015).

The seismic dilatometer SDMT is the combination of the flat dilatometer with an add-on seismic module for the measurement of the shear wave velocity V_s . The measurement system is similar to that of the SCPT. However, the SDMT uses two seismic receivers and the true-interval time can be measured, which enhances the repeatability of the V_s measurements. The seismograms recorded by the two receivers, amplified and digitized at depth, are transmitted to a PC at the surface that automatically calculates the delay using the cross-correlation algorithm, Figure 10.

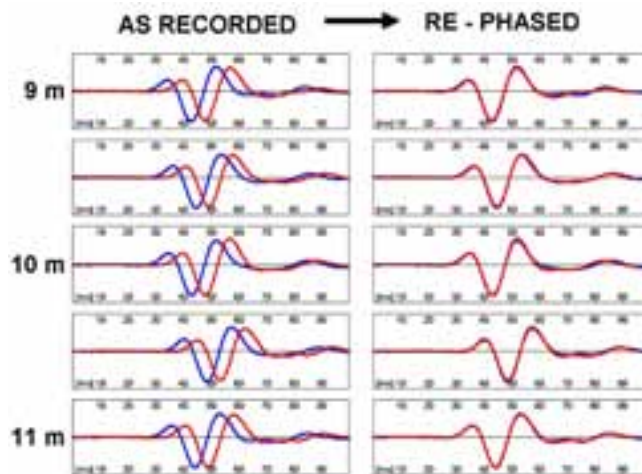


Fig. 10. Example of seismic record and re-phased signal using cross-correlation (from DMT pamphlet).

2.3 Surface Wave Methods

The most common approach used in geotechnical and earthquake engineering is called the spectral-analysis-of-surface-waves (SASW) method. The method was developed at the University of Texas at Austin and reported by Stokoe et al. (1989). Rayleigh wave energy is generated at one point and the resulting vertical surface motion is recorded at various distances (receiver points) away from the source, similar to the test set-up shown in Figure 3. Measurements are performed at multiple source-receiver spacings along a linear array. The phase shift versus frequency relationship is measured for surface waves propagating between the receivers for each receiver spacing. The result is a plot of phase velocity versus frequency for a given receiver spacing, called an individual dispersion curve. An iterative forward modeling procedure or an inversion analysis algorithm is used to determine a shear-wave velocity profile by matching the field dispersion curve with the theoretically determined dispersion curve.

The SASW method uses the apparent phase velocity dispersion curve along with source and receiver locations in the forward modeling or inversion analysis. The dynamic stiffness matrix method, which is the forward modeling algorithm used in the matching or inversion process, can simulate the apparent phase velocity specific to the source receiver configuration. The inversion analysis based on apparent phase velocities and the dynamic stiffness matrix method are key features of the SASW method, which improves the reliability and accuracy of the shear-wave velocity profile.

In the MASW method (Park et al., 1999), a large array of time traces is measured using a swept-sine vibratory source or an impulsive hammer. The basic field configuration and acquisition procedure for the MASW measurements is generally the same as the one used in conventional common midpoint (CMP) body-wave reflection surveys. In the MASW method, the dispersion curve can be determined in two approaches: the swept-frequency record approach and the frequency-wave number spectrum approach.

The MASW method uses only the fundamental mode for the inversion analysis. For the site with abnormal dispersive dispersion curve, in which phase velocities increase with increasing wavelength, the fundamental mode alone may be enough to resolve the layer stiffness reliably. To make the MASW method a reliable exploration method, it is crucial to incorporate higher modes as well as the fundamental mode in the inversion analysis. Recently, an effort to use higher modes in the inversion analysis was made by Kansas Geological Survey (Pak et al. 1999).

Note the important advantage of surface wave measurements (SASW and MASW) that reliable measurements can be performed even when wave velocities decrease with depth, or soft layers are overlain by stiff layers.

3. INTERPRETATION OF SEISMIC TESTS

3.1 Small-strain Shear Modulus

The small-strain shear modulus, G_{max} can be determined from the following relationship

$$G_{max} = V_S^2 \rho \quad (3)$$

where ρ is the bulk density of the soil. G_{max} is determined at very low shear strain, typically lower than 10^{-5} (10^{-3} %). At such a low strain level, excess pore pressure is not generated and G_{max} reflects fundamental soil behavior. As has been pointed out by Massarsch (2004), during seismic tests at shear strain level $< 10^{-3}$ %, the rate of loading (straining rate) is surprisingly slow and comparable to that of static laboratory tests. This important aspect has been confirmed by a comparison of

resonant column tests, performed at vibration frequencies of 30 to 35 Hz, and static torsional shear tests, Drnevich and Massarsch (1979). For practical purposes, the effect of strain rate on medium dense and dense granular soils can be neglected up to a strain level of approximately 0.1%.

The results of a resonant column on an undisturbed, reconsolidated sample of clayey sand is shown in Figure 11, Drnevich & Massarsch (1979). Below $10^{-3}\%$ shear strain the shear modulus appears to be unaffected by shear strain (and thus strain rate). However, when shear strains exceed $10^{-3}\%$, the shear modulus decreases. At $10^{-1}\%$ shear strain, the shear modulus of the clayey sand is only about 30% of the maximum value.

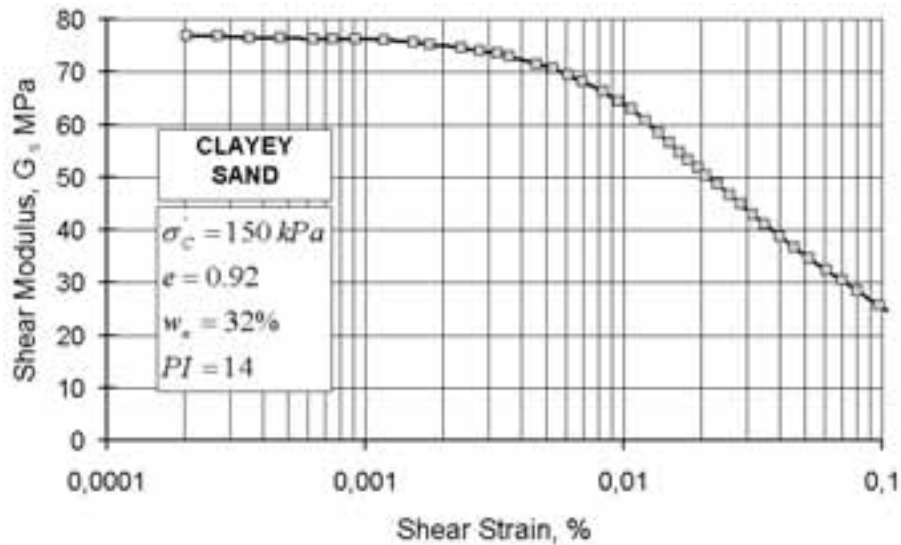


Fig. 11. Variation of shear modulus with shear strain determined from torsional resonant column test, after Drnevich and Massarsch (1979).

Based on extensive resonant column tests, Hardin (1978) suggested that the small-strain shear modulus, G_{\max} of sand can be estimated from the following relationship

$$G_{\max} = \frac{625}{0.3 + 0.7e^2} (\sigma'_m \sigma_r)^{0.5} \quad (4)$$

where: e = void ratio, σ'_m = mean effective stress and σ_r = reference stress (100 kPa). The mean effective stress σ'_m is defined as

$$\sigma'_m = \sigma'_v \left(\frac{1 + 2K_0}{3} \right) \quad (5)$$

where: σ'_v = vertical effective stress, K_0 = coefficient of lateral earth pressure at rest. Even if the horizontal stress (and thus K_0) are not known, it is preferable to estimate the coefficient of horizontal earth pressure at rest, K_0 based on engineering judgment than to neglect the significance of horizontal effective stress. Hardin (1978) found that, for granular soils, the overconsolidation ratio, OCR has little or no influence on G_{\max} . In Figure 12, the variation of the small-strain shear modulus, G_{\max} is shown for different values of the void ratio, e as a function of the mean effect

stress, σ'_m . It is assumed that the groundwater table is at the ground surface, the coefficient of lateral earth pressure at rest, K_0 , is 0.5, and the bulk density, ρ , is 2000 kg/m³.

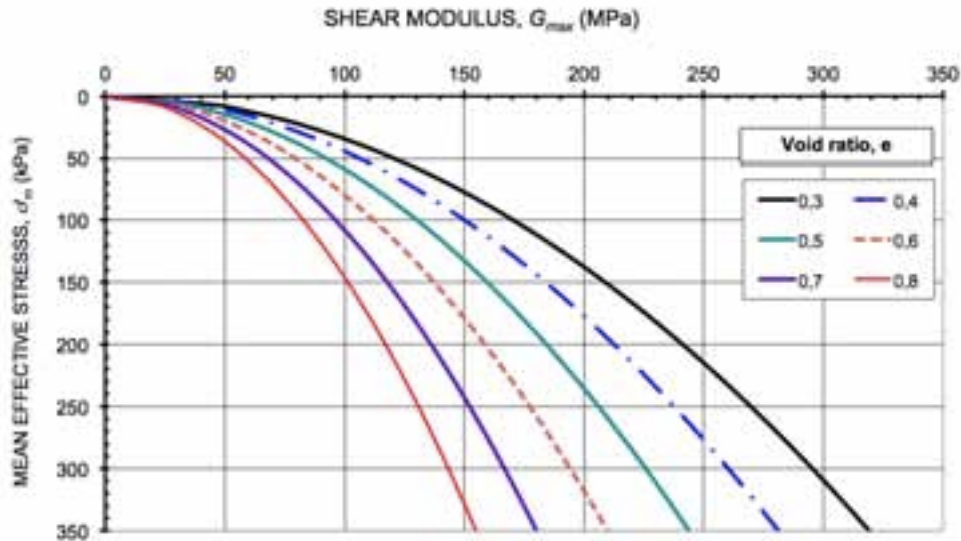


Fig. 12. Variation of the small-strain shear modulus with mean effective stress for different values of void ratio, cf. Equation (5). The ground water level is assumed at the ground surface.

3.2 Modulus Degradation of Fine-grained Soils

The shear modulus decreases with increasing shear strain level, cf. Figure 11. The static shear modulus, G_s (defined as shear modulus at a shear strain level of approximately 0.5 % shear strain, which corresponds to working load at a factor of safety, $FS > 1.5$) can be estimated from the following relationship

$$G_s = R_M G_{max} \quad (6)$$

where: R_M = modulus reduction factor, G_{max} = shear modulus at small strain ($<10^{-3}\%$). The modulus reduction factor, R_M of fine-grained soils has been investigated by Massarsch (2004). Based on the evaluation of extensive resonant column test data, a relationship was found which describes the variation of the normalized shear modulus is shown as a function of shear strain, for different values of PI , Figure 13. It is apparent that shear modulus degradation is more pronounced with decreasing plasticity index, PI .

The effect of basic soil parameters on the modulus reduction factor, R_M of silts and sands, such as plasticity index, PI , void ratio, e , and degree of saturation, S_r , has been investigated by Massarsch (2015).

A robust relationship for fine-grained soils between R_M at 0.5 % shear strain and plasticity index, PI , has been proposed by Massarsch (2004). The relationship between R_M and PI is shown in Figure 14 for PI values ranging from 0 to 100 %. The following relationship between the modulus reduction factor, R_M , and plasticity index, PI , is obtained

$$R_M = 0.0043 PI + 0.103 \quad (7)$$

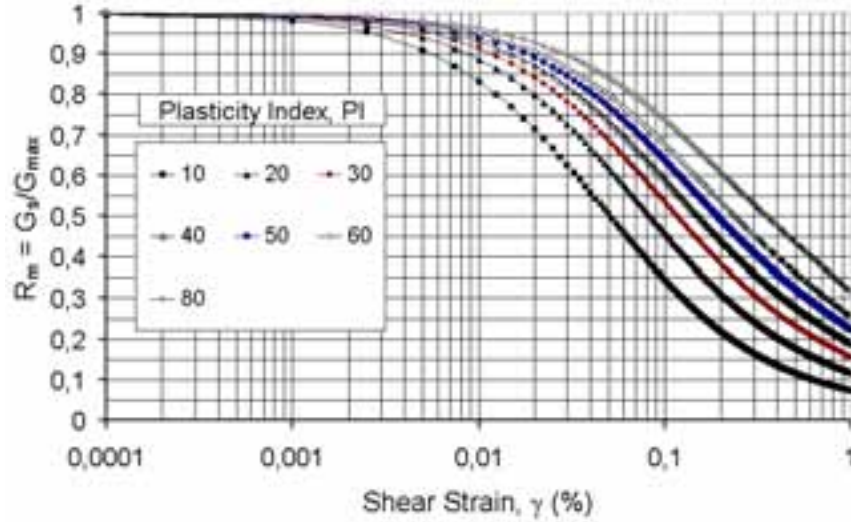


Fig. 13. Variation of the normalized shear modulus as a function of shear strain for different values of PI , Massarsch (2004).

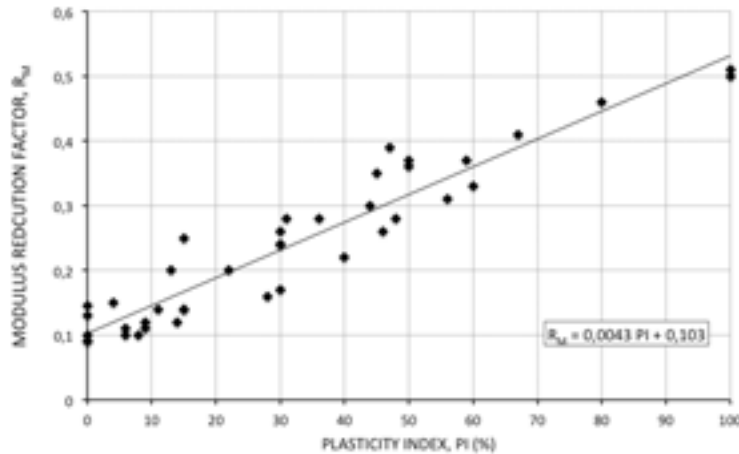


Fig. 14. Relationship between modulus reduction factor, R_M and plasticity index, PI including data from Table 2 and results by Massarsch (2015).

For granular soils, the dependence of R_M on void ratio, e , is shown in Figure 15, from which the following relationship between void ratio, e , and the modulus reduction factor, R_M , is obtained

$$R_M = 0.111e + 0.063 \quad (8)$$

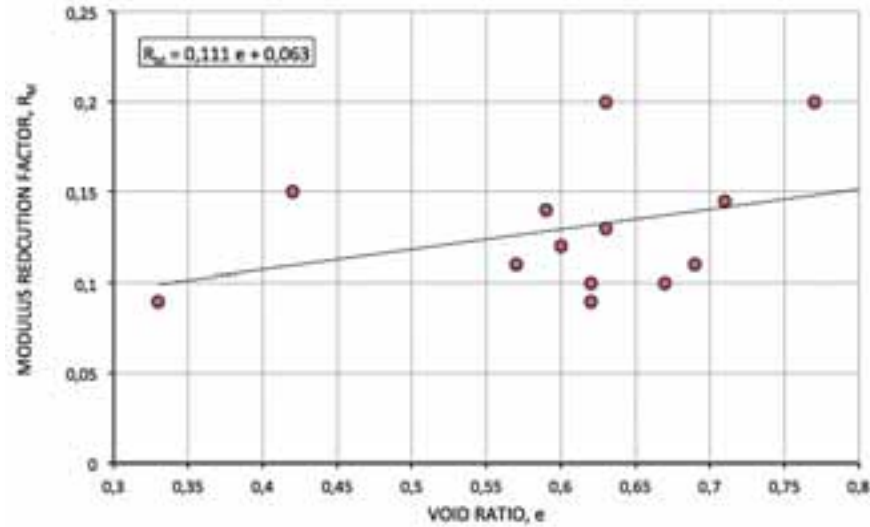


Figure 15. Variation of modulus reduction factor R_M (0.5 % shear strain) with void ratio in silt and sand, (Massarsch 2015).

In spite of some scatter in the data, it is apparent that the modulus reduction effect is more pronounced in dense (low void ratio) than in loose (high void ratio) granular soils. On average, G_{max} decreases at a shear strain level of 0.5 % to between 10 and 15 % of the maximum value. For a void ratio between $e = 0.3$ and 0.8 , R_M varies between 0.096 and 0.152. On average, in medium dense (compact) sand with a void ratio $e = 0.60$, R_M is 0.13. The relative density of sands can be approximately characterized by the ranges of void ratio shown in Table 2.

TABLE 2. Approximate range of values for void ratio in sand with different densities (Massarsch 2015).

Density	Void Ratio, e
Very dense	0.35 – 0.45
Dense	0.45 - 0.55
Compact	0.55 – 0.65
Loose	0.65 – 0.75
Very loose	0.75 – 0.85

The dependence of the modulus reduction factor on the degree of saturation is shown in Figure 16. There is scatter in the data at high degree of saturation, but the trend shows that S_r has only a slight effect on R_M .

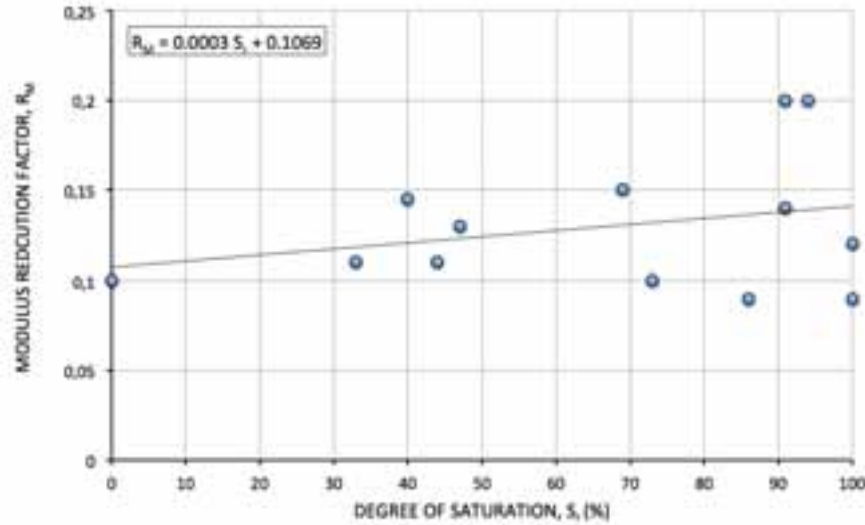


Fig. 16. Variation of modulus reduction factor R_M at 0.5 % shear strain with degree of saturation.

From Figures 16, the effect of the degree of saturation on the modulus reduction factor can be determined from the following equations

$$R_M = 0.0003 S_r + 0.1069 \quad (9)$$

A slight increase of the modulus reduction factor appears to occur with increasing degree of saturation. For most soils the average value of R_M can be assumed to be 0.13, a value similar to that of the void ratio. However, for most practical purposes, the influence of S_r on R_M can be neglected.

3.3 Relationship between Moduli

It is recommended to determine the elastic (Young's) modulus, E , and the constrained modulus, M , from the shear modulus G (at strain level ≈ 0.5 % shear strain).

$$E = 2(1 + \nu)G \quad (10)$$

$$M = \frac{(1-\nu)}{(1-2\nu)(1+\nu)}E = \frac{2(1-\nu)}{(1-2\nu)} G \quad (11)$$

It should be noted that Poisson's ratio, ν is strain dependent and increases with increasing strain level. The ratio between different moduli for a range of values of Poisson's ratio, ν is shown in Table 3.

The variation of the elastic modulus, E as a function of mean effective stress can be determined by substituting Equation (5) into Equation (11). For sand an average value $R_M = 0.13$ is chosen. Assuming that the ground water table is located at the ground surface, Poisson's ration, $\nu = 0.30$, unit weight $\rho = 20 \text{ kN/m}^3$ and coefficient of lateral earth pressure at rest, $K_0 = 0.5$, the elastic modulus, E at 0.5% shear strain (i.e. "static modulus") can be determined. The variation of elastic

modulus as a function of mean confining stress and for different values of void ratio is shown in Figure 17.

TABLE 3. Modulus ratio for values of Poisson’s ratio, ν , cf. Eq. (10) and (11).

Poisson's ratio	E/G	M/G	M/E
0.25	2.50	3.00	1.20
0.30	2.60	3.50	1.35
0.33	2.66	3.94	1.48
0.40	2.80	6.00	2.14
0.49	2.98	51.00	17.11

For example, in granular soils ($\nu = 0.30$), the elastic modulus $E = 2.6 G$ and the confined modulus $M = 3.5 G$. The variation of the elastic modulus, E as a function of mean effective stress can be determined by substituting Equation (5) into Equation (11). For sand an average value $R_M = 0.13$ is chosen. Assuming that the ground water table is located at the ground surface, Poisson’s ratio, $\nu = 0.30$, unit weight $\rho = 20 \text{ kN/m}^3$ and coefficient of lateral earth pressure at rest, $K_0 = 0.5$, the elastic modulus, E at 0.5% shear strain (i.e. “static modulus”) can be determined. The variation of elastic modulus as a function of mean confining stress and for different values of void ratio is shown in Figure 17.

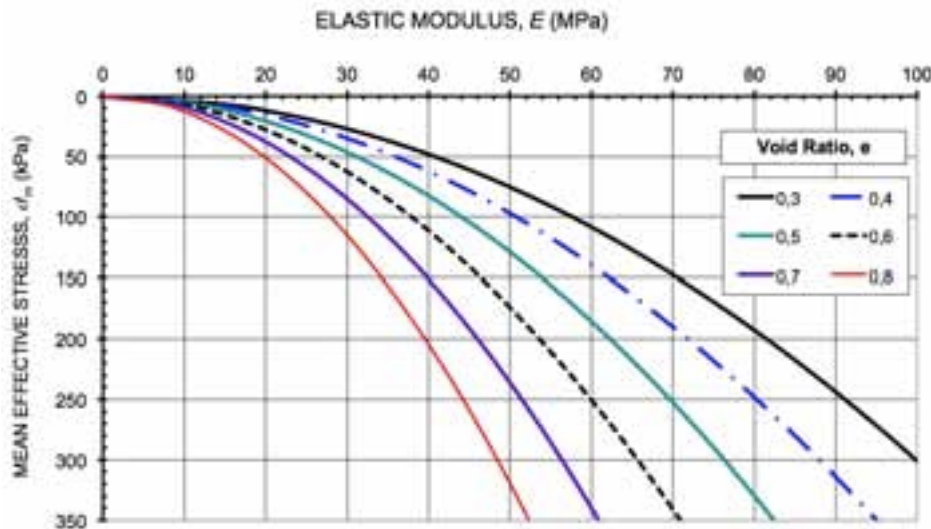


Fig. 17. Dependence of elastic modulus, E , at 0.5% shear strain on mean confining stress as a function of void ratio, e .

4. RESULTS OF SEISMIC MEASUREMENTS

As described above, three different types of seismic measurements have been performed, comprising: seismic refraction, surface wave measurement ($MASW$) and seismic downhole tests ($SCPT$ and $SDMT$). Seismic refraction and $MASW$ measurements and interpretation of data was carried out by WARNES, Santa Cruz and $SCPT$ and $SDMT$ tests by Incotec, respectively. A large

number of tests have been which will be made available as part of the B.E.S.T. project. Typical results along the test area have been chosen and are presented below.

4.1 Seismic Refraction

The seismic refraction measurements are two-dimensional along a 92 m long profile, cf. Figure 2. Compression waves were generated by means of hammer blows on the ground surface. The results are presented in a tomographic image of compression waves (V_p) and are compared to the cone stress measurement in test point C1, Figure 18.

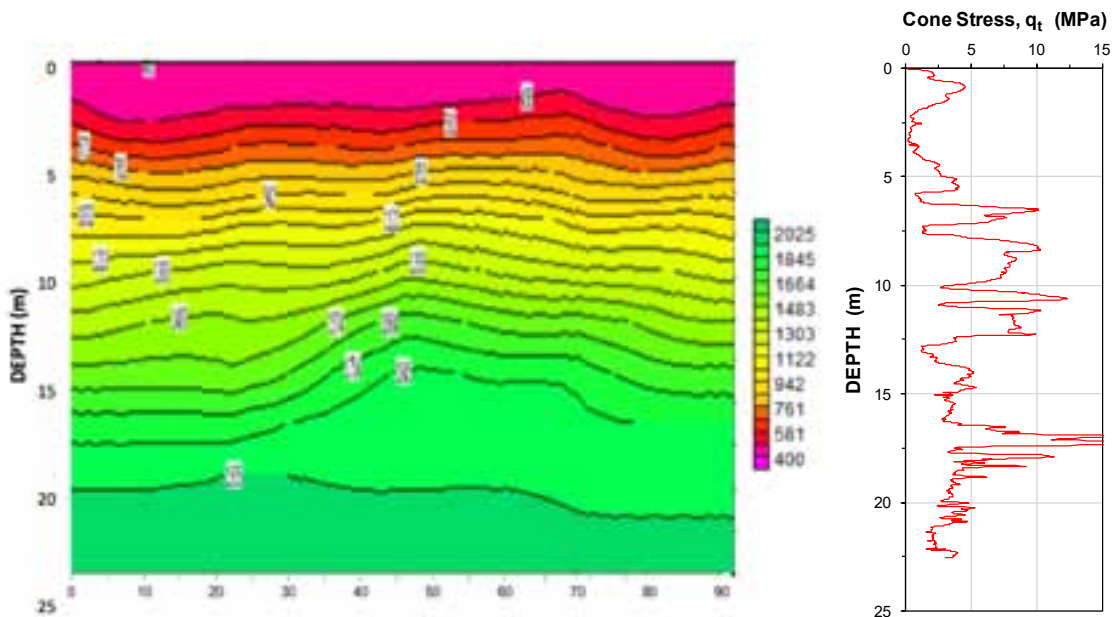


Fig. 18. Result of seismic refraction measurement, variation of compression wave velocity, V_p along Line B and comparison with CPT C1, cf. Figure 2.

The image indicates a relatively homogenous medium with generally horizontal layers and a final refractive boundary at approximately 20.0 m. The first layer down to approximately 5 m depth shows a P -wave velocity of 400 to 750 m/s. The subsequent layer (5 to 8 m) has a P -wave velocity of 750 to 1,300 m/s. Below follows a layer (8 to 20 m) with gradually increasing P -wave velocity (1,300 m/s to 1,900 m/s). At 20 m depth, a stiff boundary was detected.

As mentioned above, seismic refraction cannot detect soil layers, which are overlain by a high velocity layer. Thus it is not surprising, that the compressible layer between 12 and 16 m is not detected. The groundwater table is located close to the ground surface. In water-saturated soils, the P -wave velocity is approximately 1,450 m/s. Thus, the P -wave velocity down to about 10 m depth is underestimated. It can be concluded that seismic refraction gives a qualitative representation of soil strata, but is not suitable for geotechnical applications.

4.2 Surface Wave Measurement

Surface wave measurements can be carried out in soil deposit with varying wave velocity profiles. Multichannel Analysis of Surface Waves (MASW) was carried out along two profiles, A and C, cf., Figure 3. Rayleigh waves were generated by a hammer blow and surface waves were recorded

along two profiles. The results of the MASW investigations are shown in Figure 19 and 20. Also shown is the variation of cone stress with depth, cf. Figure 3.

It should be noted that the distance between Locations A and C is 6 m. Thus, the two profiles should give similar results, considering the homogeneity of the site. Both profiles show similar results, with shear wave velocities increasing generally with depth, from about 150 m/s near the ground surface, to 180 m/s at 5 m depth. The stiffer layer between 5 and 12 m is also detected, with an average shear wave velocity of 200 m/s, followed by a layer with higher wave velocity. However, in profile C, a layer is detected with lower velocity (200 m/s) is found embedded in the soil layer with higher velocity (220 m/s).

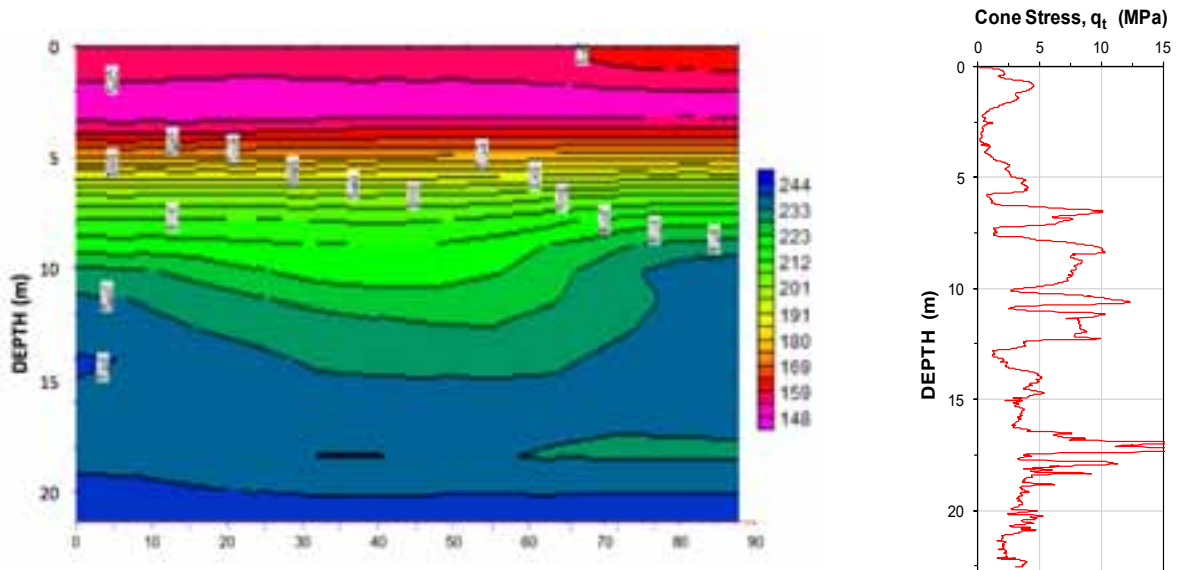


Fig. 19. Result of MASW measurement, variation of shear wave velocity, V_s along Line A and comparison with CPT C1, cf. Figure 2.

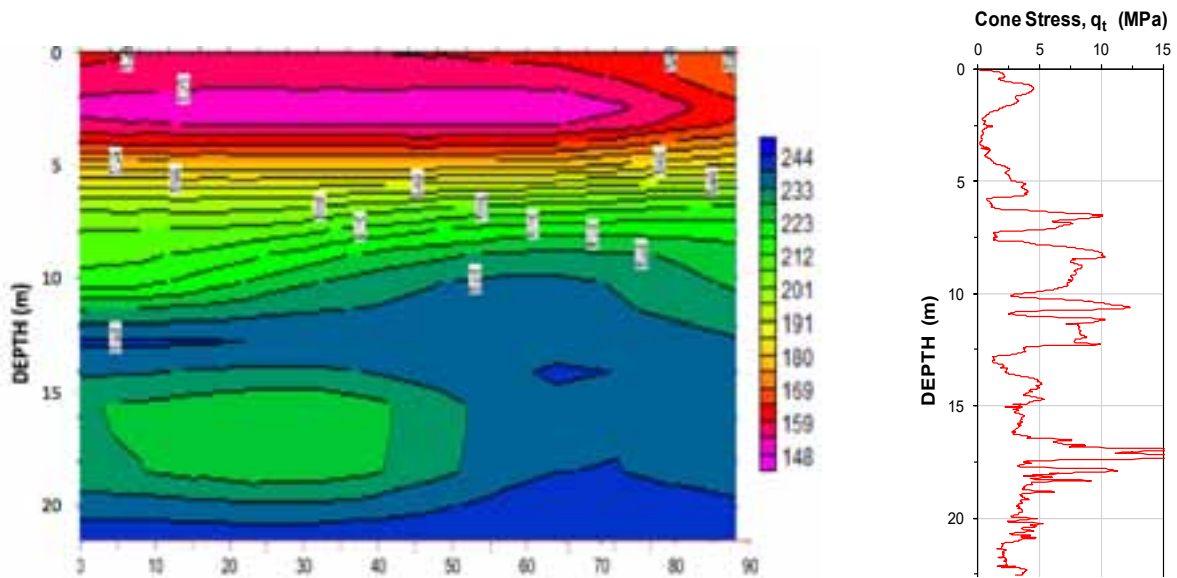


Fig. 20. Result of MASW measurement, variation of shear wave velocity, V_s along Line C and comparison with CPT C1, cf. Figure 2.

Based on the seismic refraction and surface wave measurements, a soil profile was established, independent prior to the geotechnical investigations which were performed at a later stage of the project. Figure 21 shows a generalized soil profile with a color code according to Table 4. Also shown is the CPT in test point C1.

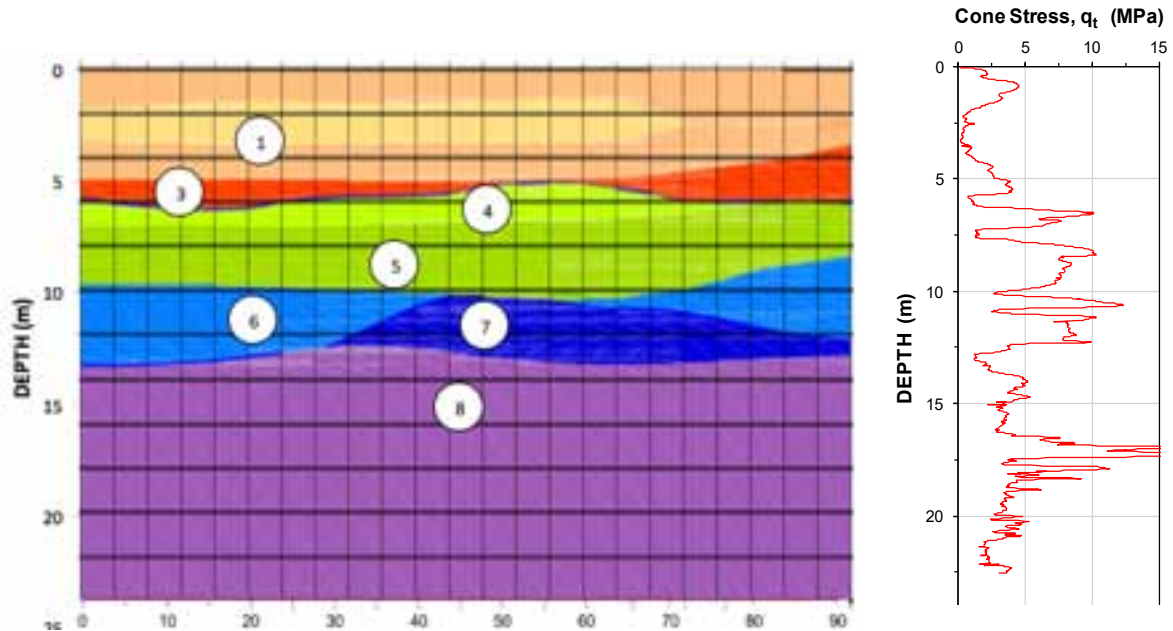


Fig. 21. Generalized soil profile based on seismic refraction and MASW investigations. Also shown is CPT C1. Soil layers and wave velocities are identified in Table 4.

TABLE 4. Identification of soil layers along profile A, B and C, based on refraction and surface wave measurements.

Seismic Units	Pattern	V_P (m/s)	V_S (m/s)
1		400	<155
2		400	155 - 175
3		400	175 - 200
4		1500	200 - 225
5		1500	225 - 240
6		1500	240 - 225
7		1500	225 - 240
8		1700	> 240

4.3 Seismic Down-hole Tests

Two different types of seismic down-hole tests were performed. The SCPT tests used only one seismic sensor, cf. Figure 5a, while the SDMT used two seismic sensors, cf. Figure 5b. There were also differences in the method of analysis. In the case of SCPT, the first arrival time at different levels was determined by picking peak values in the time-history trace, a method which is subject to some uncertainty. In contrast, for the analysis of SDMT data, cross-correlation (phase shift

method) was used to determine the time difference between wave arrivals at two separated locations.

Figure 22 shows the determined shear wave velocities by the SCPT and SDMT method at three locations along the test area. In general, the agreement between the two tests is good. However, it is apparent that the S-wave velocities determined by the SCPT (one seismic sensor) fluctuate significantly, especially at depths exceeding about 10 m.

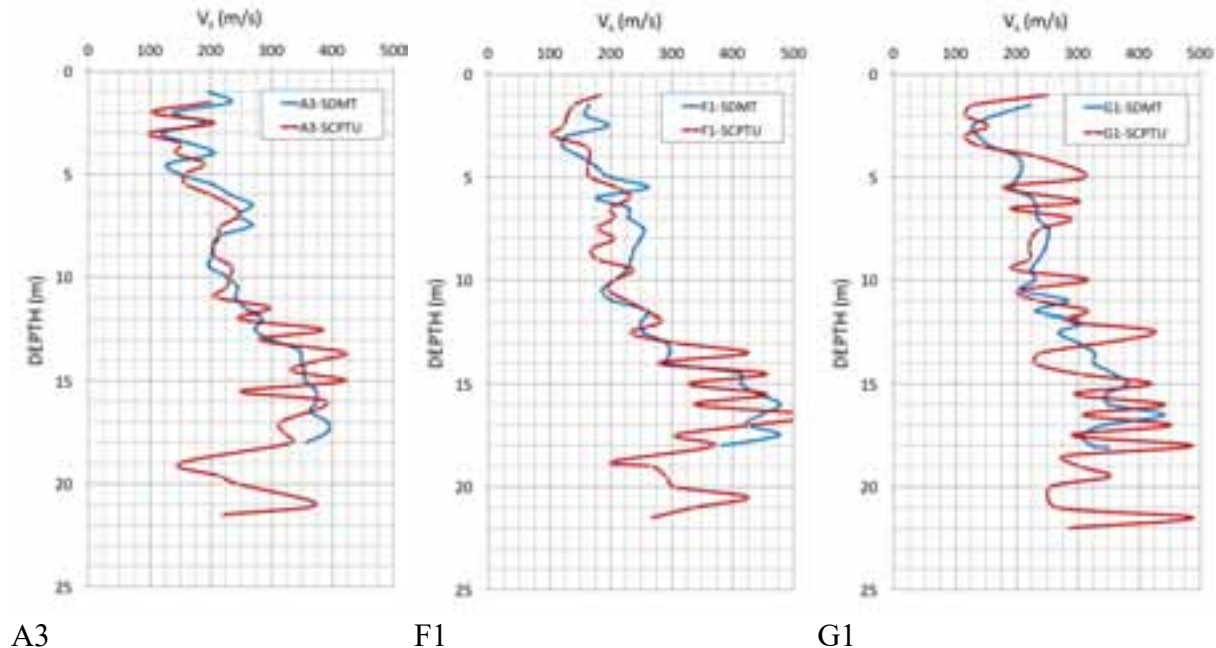


Fig. 22. Results of SDMT and SCPT measurements in three locations along the test area, cf. Figure 3.

Figure 23 compares shear wave velocities measured by down-hole tests (SCPT and SDMT) with the surface wave velocity (MASW) measurements. The general agreement between the average values of down-hole tests and MASW tests is fair. The down-hole method provides significantly more detailed resolution, especially in the case of the SDMT data.

5. DETERMINATION OF SOIL MODULUS

In geotechnical engineering, an important application of seismic measurements is the determination of the deformation properties (moduli) of soils and rock. Section 3 outlines concepts which can be used to determine, based on shear wave velocity measurements, the small-strain shear modulus, G_{\max} and the large-strain (static) shear modulus, G_s , respectively. As has been shown in the previous section, the shear wave velocity determined by the *SDMT* gives the most consistent results. Therefore, the shear modulus at small strain, G_{\max} , and the static shear modulus (at 0.5 % shear strain) has been determined only based on *SDMT* results, cf. Figure 24. The unit weight of the different soil layers was based on the interpretation of CPUT and laboratory tests, where available. The static shear modulus was calculated based on Eqs. (7) and (8). On average, the modulus reduction factor, RM, varied between 0.10 (sand) and 0.20 (clayey silt).

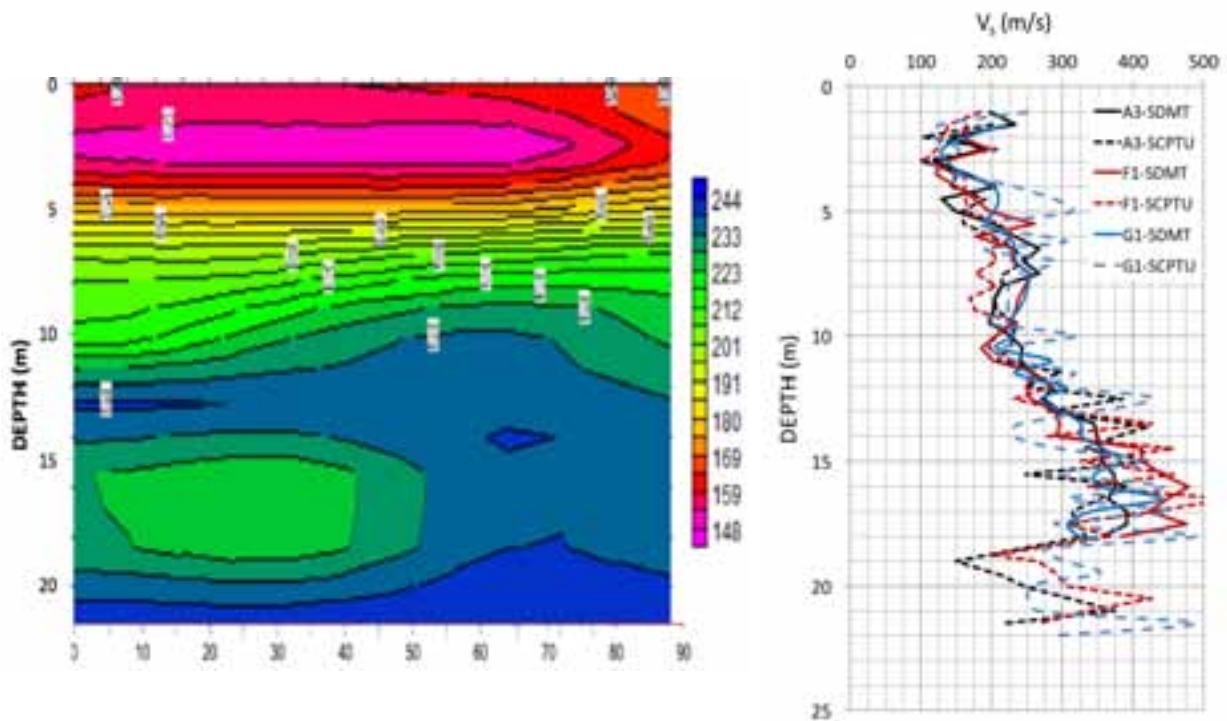


Fig. 23. Comparison of results from down-hole tests (SDMT and SCPT) and MASW measurements in three locations along the test area, cf. Figure 17.

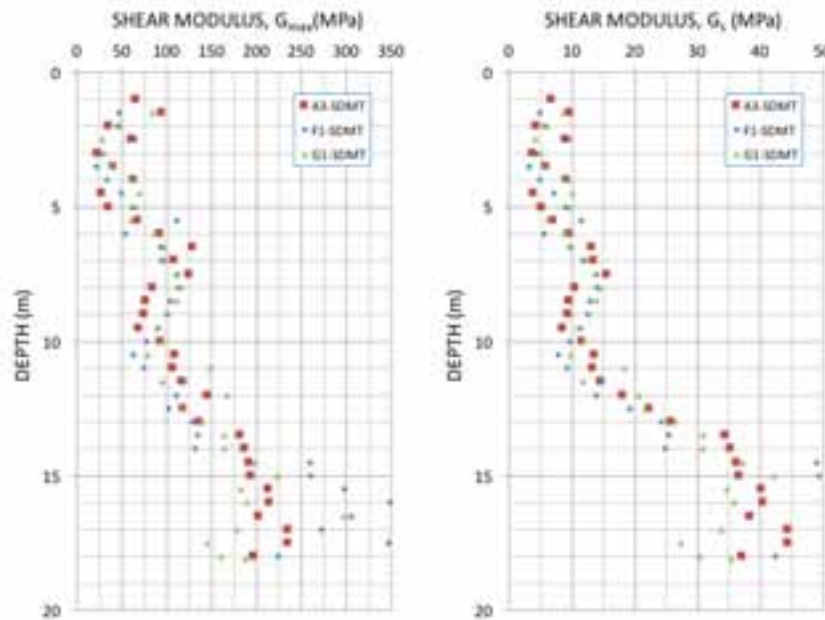


Fig. 24. Small-strain shear modulus, G_{max} and static shear modulus, G_s (0.5 % shear strain) determined from SDMT results in test locations A3, F1, and G1.

It should be observed that an error in the measurement of the shear wave velocity will be magnified when calculating the shear modulus, cf. Eq. (3). For example, an error in the shear wave velocity of 25 % will result in an error in the shear modulus of 56 %!

Figure 25 shows the small-strain modulus, G_{max} and the derived static moduli (0.5 % shear strain), G_s and E_s , respectively for the three test locations, A, F, and G. It can be observed that the soil moduli vary both in the lateral direction (from A to G) as well as with respect to depth.

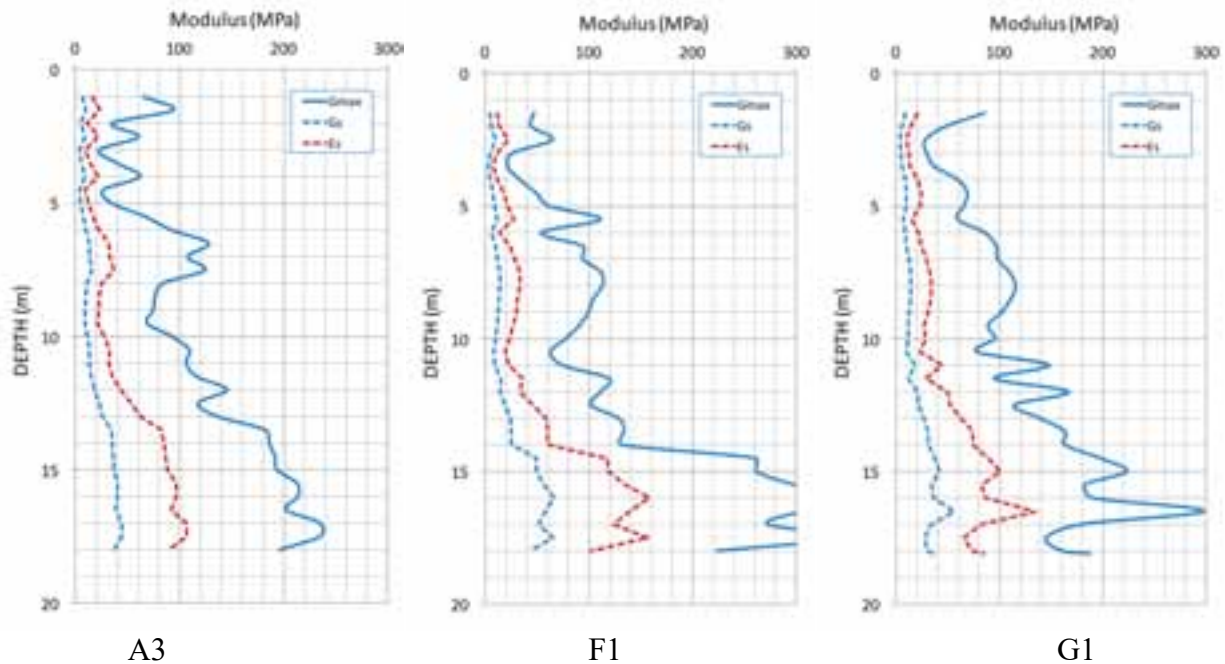


Fig. 25. Small-strain shear modulus, G_{max} and static shear modulus, G_s (0.5 % shear strain) and E_s at three test locations (A, F and G).

6. SUMMARY AND CONCLUSIONS

The geotechnical and seismic investigations at the B.E.S.T. site with relatively homogeneous soil conditions provide a unique opportunity to compare the results of different testing methods. A large number of tests has been carried out at well-defined investigation points.

As seismic testing is still not considered part of geotechnical routine investigations, the paper describes the fundamentals of the three methods used at the B.E.S.T. site: seismic refraction, surface wave (MASW), and down-hole test (SCPT and SDMT). Seismic testing methods are well-established and described in guidance documents and standards. Of particular importance is that the tests are performed with diligence as even minor deviations can lead to significant errors. Another important aspect is the method of data interpretation. With the increasing computational power and the availability of advanced analytical methods, the quality of data evaluation has improved significantly in the recent past. An example of this development is the application of surface wave measurements (SASW and MASW).

Probably the most important aspect of seismic testing for geotechnical applications is the derivation of soil stiffness (modulus) based on shear wave velocity measurements. Therefore, a significant part of the paper is devoted to the description of a practically applicable concept of calculating the static soil modulus corresponding to a shear strain level of 0.5 %.

The results of seismic measurements are presented and compared with geotechnical information, based on CPTU. Also, the results from different testing methods are compared. Based

on the shear wave velocity, V_s the shear modulus at small strain, G_{\max} and the corresponding static moduli G_s and E can be calculated.

From the results presented above, it can be concluded that the most reliable method of seismic field testing is the down-hole method, using two seismic sensors. Data interpretation should be carried out using a reliable, interpreter-independent method, such as cross-correlation (phase shift method).

7. REFERENCES

- Butcher, A. P., Campanella, R.G., Kaynia, A.M. and Massarsch, K. R., 2015. Seismic cone downhole procedure to measure shear wave velocity - a guideline prepared by ISSMGE TC10: Geophysical Testing in Geotechnical Engineering. XVIth International Conference on Soil Mechanics and Geotechnical Engineering, Osaka, published in ISSMGE News 2015, ISSMGE Bulletin, 9(2) 17-26.
- Drnevich, V. P. and Massarsch, K. R. (1979). Sample Disturbance and Stress - Strain Behaviour, ASCE Journal of the Geotechnical Engineering Division, 105(GT 9) 1001-1016.
- Hardin, B. (1978). The nature of stress strain behaviour of soils. Proceedings, ASCE Specialty Conference on Earthquake Engineering and Soil Dynamics, Pasadena, Vol. 1. pp. 3 – 30.
- Massarsch, K. R. 2004. Deformation properties of fine-grained soils from seismic tests. Keynote lecture, International Conference on Site Characterization, ISC'2, 19 – 22 Sept. 2004, Porto, pp. 133-146.
- Massarsch, K.R. 2015. Determination of shear modulus of soil from static and seismic penetration testing. Jubilee Volume. Proceedings in honour of Prof. A. Anagnostopoulos, Technical University of Athens, School of Civil Engineering – Geotechnical Department. Ed. M. Kavvas. Athens 2015. Publisher: Tsotras ISBN: 978-618-5066-30-7, pp. 335 - 352.
- Park, C.B., Miller, R.D., and Xia, J., 1999, Multichannel analysis of surface waves (MASW). Geophysics, Vol. 64, pp. 800-808.
- Richart, F.E., Jr., Hall, J.R. and Woods, R.D. 1970. Vibrations of Soils and Foundations. Englewood Cliffs, New Jersey, Prentice Hall, 414 p.
- Robertson, P.K., Campanella, R.G., Gillespie, D. and Rice, A. 1986. Seismic CPT to Measure In-Situ Shear Wave Velocity. ASCE, Journal of Geotechnical Engineering, 112(8) 791-804.
- Santamarina, J. C., Klein, K.A., and Fam, M.A. 2001. Soils and Waves. John Wiley & Sons, Ltd., Rexdale, Ontario, Canada, 488 p.
- Stokoe, K.H., Rix, G.J. and Nazarian, S. 1989. In-situ seismic testing with surface waves. International Conference on Soil Mechanics and Foundation Engineering, Rio de Janeiro, August 1989. Proceedings, Vol. 1. pp. 331-334.
- Stokoe, K.H., II, Joh, S.H. and Woods, R.D. 2004. Geotechnical and geophysical site characterization. International conference on site characterization, 2, ISC 2, Porto, Portugal, 19-22 September, 2004. Proceedings, Vol. 1, pp. 97-132.
- Youd, T. L., Idriss, I. M., Andrus, R. D., Arango, I., Castro, G., Christian, J.T., Dobry, R., Liam Finn, W.D., Harder Jr.L.F., Hynes, M.E., Ishihara, K., Koester, J.P., Liao, S.S.C., Marcuson III, W.F., Martin, G.R., Mitchell, J.K., Moriwaki, Y., Power, M.S., Robertson, P.K., Seed, R.B., and Stokoe II, K.H., 2001. Liquefaction Resistance of Soils: Summary Report from the 1996 NCEER and 1998 NCEER/NSF Workshops on Evaluation of Liquefaction Resistance of Soils. Journal of Geotechnical and Geoenvironmental Engineering, ASCE, 127(10) 817-833.